# Supporting Information

# Metal Decoration of Si Particles via High-Energy Milling for Lithium-ion Battery Anodes

*Khryslyn G. Araño[1*], Beth L. Armstrong[2], Robert L. Sacci[1], Matthew S. Chambers[1], Chun-Sheng Jiang[3], Joseph Quinn[4], Harry M. Meyer III[1], Anton W. Tomich[5], Amanda Musgrove[1], Steven Lam[1], Elena Toups[1], Chongmin Wang[4], Christopher S. Johnson[5], Gabriel M. Veith[1*]*

[1]Chemical Sciences Division, Oak Ridge National Laboratory, Oak Ridge, Tennessee 37831, United States

[2]Materials Science and Technology Division, Oak Ridge National Laboratory, Oak Ridge, Tennessee 37831, United States

[3]Materials Science Center, National Renewable Energy Laboratory, Golden, Colorado 80401, United States

[4]Environmental Molecular Sciences Laboratory, Pacific Northwest National Laboratory, Richland, Washington 99354, United States

[5]Chemical Science and Engineering Division, Argonne National Laboratory, 9700 South Cass Avenue, Argonne Illinois 60439-4837, United States

Corresponding authors email address:

Khryslyn G. Araño: khryslyn.arano@gmail.com

Gabriel M. Veith: veithgm@ornl.gov

## XRD Analysis of the Si Powder

**Table S1.** Starting models used in Rietveld refinement.

| Model | Reference |
|---|---|
| Si | Többens *et al.*[1] |
| Ag | Swathi *et al.*[2] |
| Al | Didier *et al.*[3] |
| Fe | Kohlhaas *et al.*[4] |
| Ni | Conway & Prior *et al.*[5] |
| Ti | Wasilewski *et al.*[6] |
| Y | Spedding *et al.*[7] |

**Table S2.** Fitting parameters for the Rietveld refinement of the metal-decorated Si powders.

| Material | $R_{wp}$ | $\chi^2$ |
|---|---|---|
| $Si^{Ag}$ | 9.996% | 2.642 |
| $Si^{Al}$ | 8.520% | 2.385 |
| $Si^{Fe}$ | 2.867% | 1.323 |
| $Si^{Ni}$ | 3.616% | 2.095 |
| $Si^{Ti}$ | 10.137% | 2.486 |
| $Si^{Y}$ | 9.145% | 2.933 |

**Table S3.** $Si^{M}$ cell parameters.

| **Sample** | **Si cell parameter (Å)** |
|---|---|
| $Si^{Ag}$ | 5.4302(3) |
| $Si^{Al}$ | 5.43059(14) |

| | |
|---|---|
| $Si^{Fe}$ | 5.43299(16) |
| $Si^{Ni}$ | 5.4302(3) |
| $Si^{Ti}$ | 5.4330(2) |
| $Si^{Y}$ | 5.4299(3) |
| Si | 5.4311(5) |

## Scanning Electron Microscopy

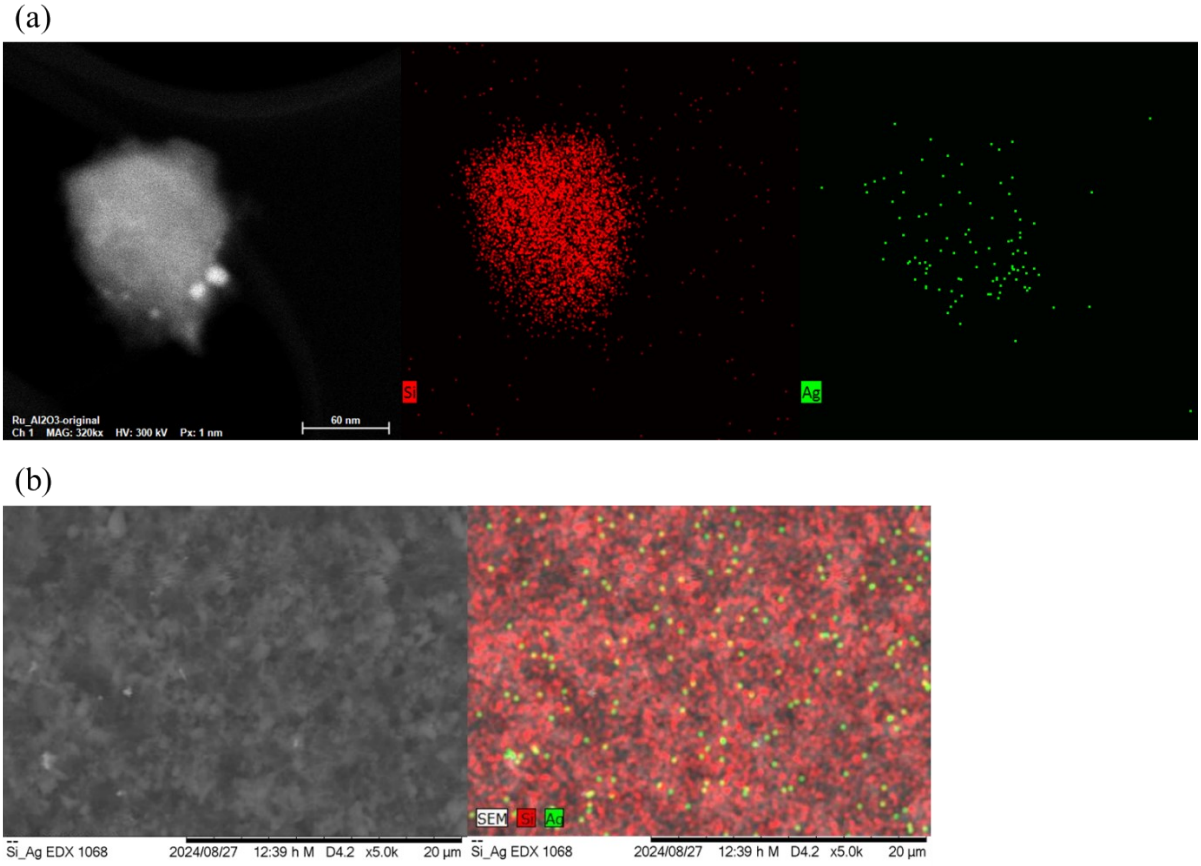


**Figure S1.** a) TEM images of the $Si^{Ag}$ particle and b) surface SEM-EDX images of the pristine $Si^{Ag}$ electrode.

## Scanning Spreading Resistance Microscopy (SSRM) of the Electrodes

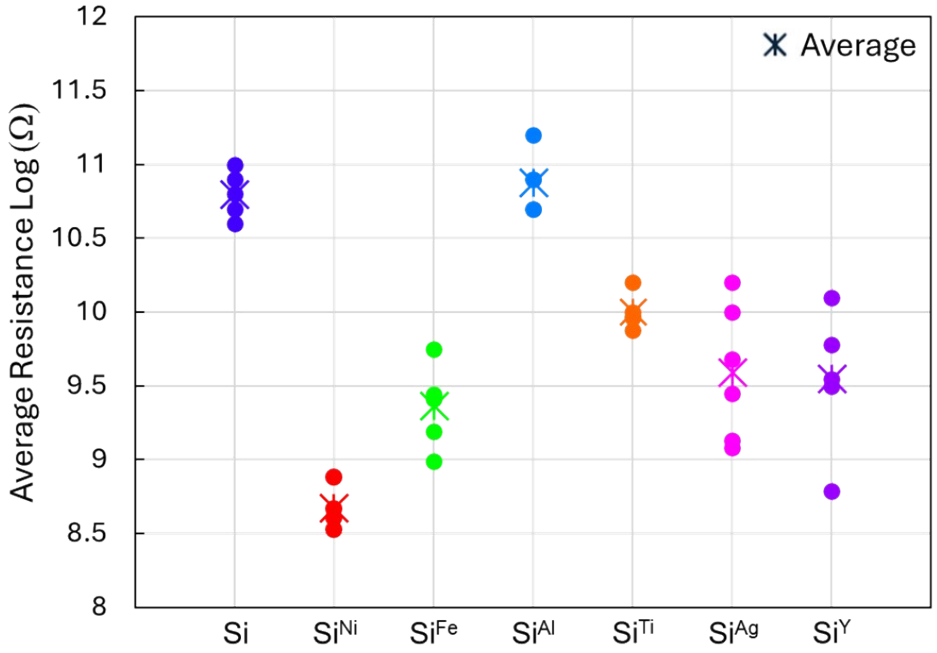


**Figure S2.** Average resistance of the electrodes prepared from the baseline Si and metal-decorated Si powders obtained from SSRM-AFM measurements.

## Electrochemical Tests of the $Si^M$ Electrodes

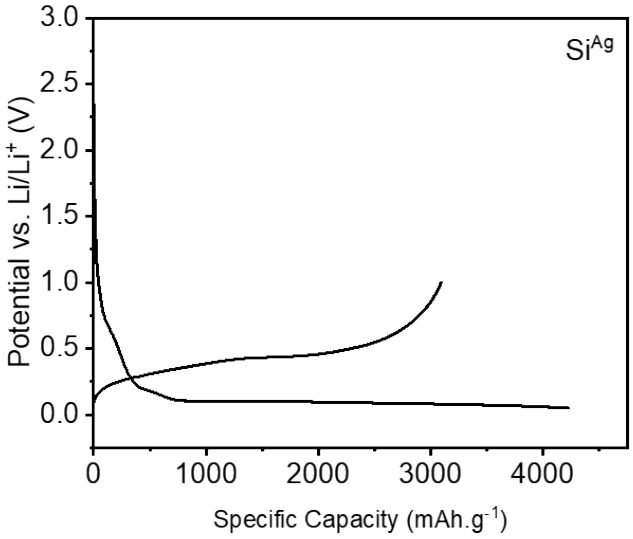


**Figure S3.** First cycle half-cell charge-discharge profile of $Si^{Ag}$.

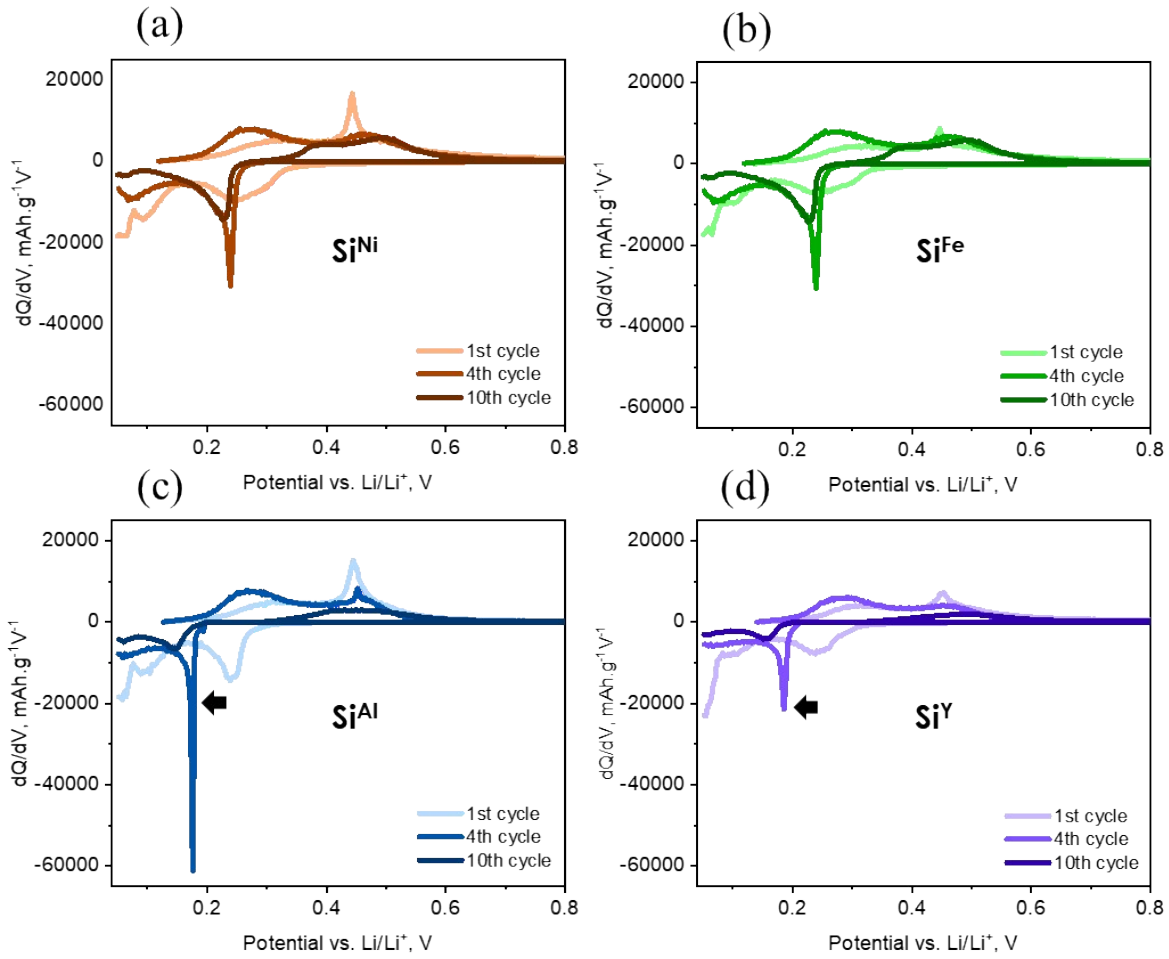


**Figure S4.** Voltage profiles of a) $Si^{Ni}$, b) $Si^{Fe}$, c) $Si^{Al}$, and d) $Si^{Y}$ during cycling in half-cell configuration.

**Table S4.** Coulombic efficiencies of the $Si^{M}$ half cells.

| | 20th Cycle | 40th Cycle | 60th Cycle | 80th Cycle | 100th Cycle |
|---|---|---|---|---|---|
| **Baseline Si** | 100% | 99.8% | 99.2% | 99.0% | 99.7% |
| **$Si^{Fe}$** | 100% | 100% | 100% | 99.7% | 99.4% |
| **$Si^{Ni}$** | 100% | 99.8% | 99.6% | 99.3% | 99.3% |
| **$Si^{Ti}$** | 100% | 98.9% | 98.5% | 98.2% | 98.5% |
| **$Si^{Ag}$** | 99.7% | 99.7% | 99.7% | 99.6% | 99.5% |
| **$Si^{Al}$** | 99.2% | 100% | 99.9% | 99.6% | 99.5% |
| **$Si^{Y}$** | 99.6% | 99.2% | 99.4% | 99.6% | 99.8% |

## Electrochemical Impedance Spectroscopy Measurements in Half Cells

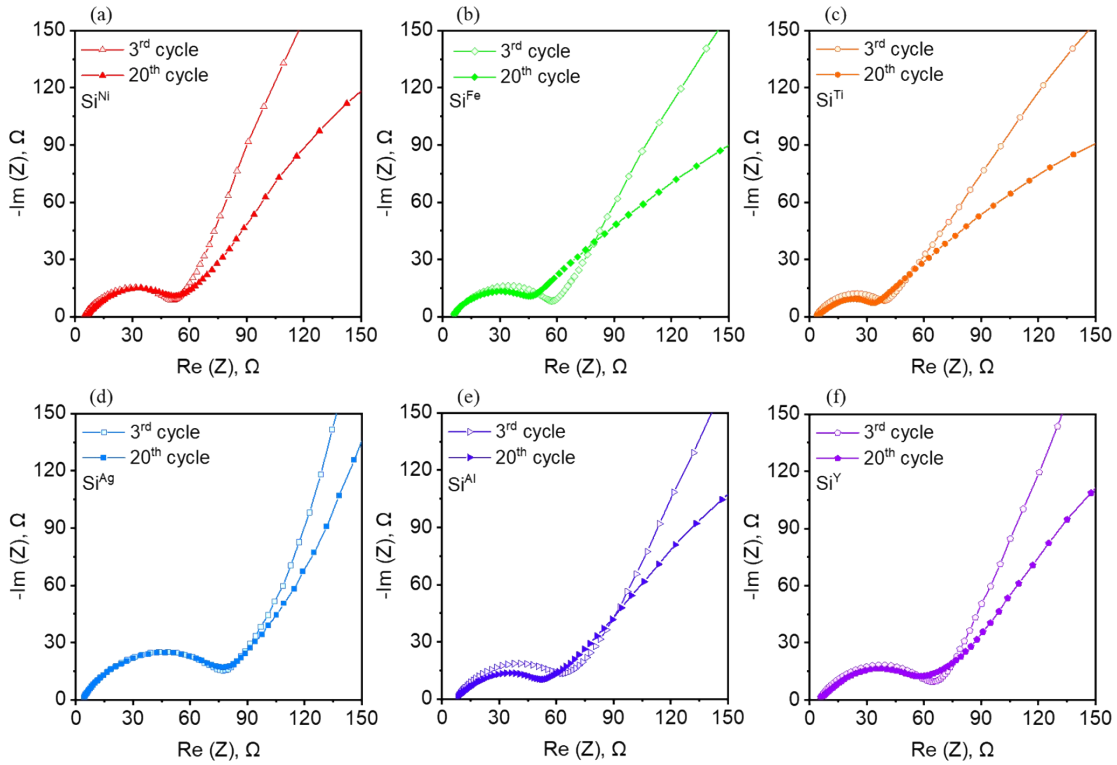


**Figure S5.** Nyquist profiles of a) $Si^{Ni}$, b) $Si^{Fe}$, c) $Si^{Ti}$, d) $Si^{Ag}$, e) $Si^{Al}$, and f) SiY at delithiated states in half-cell configuration

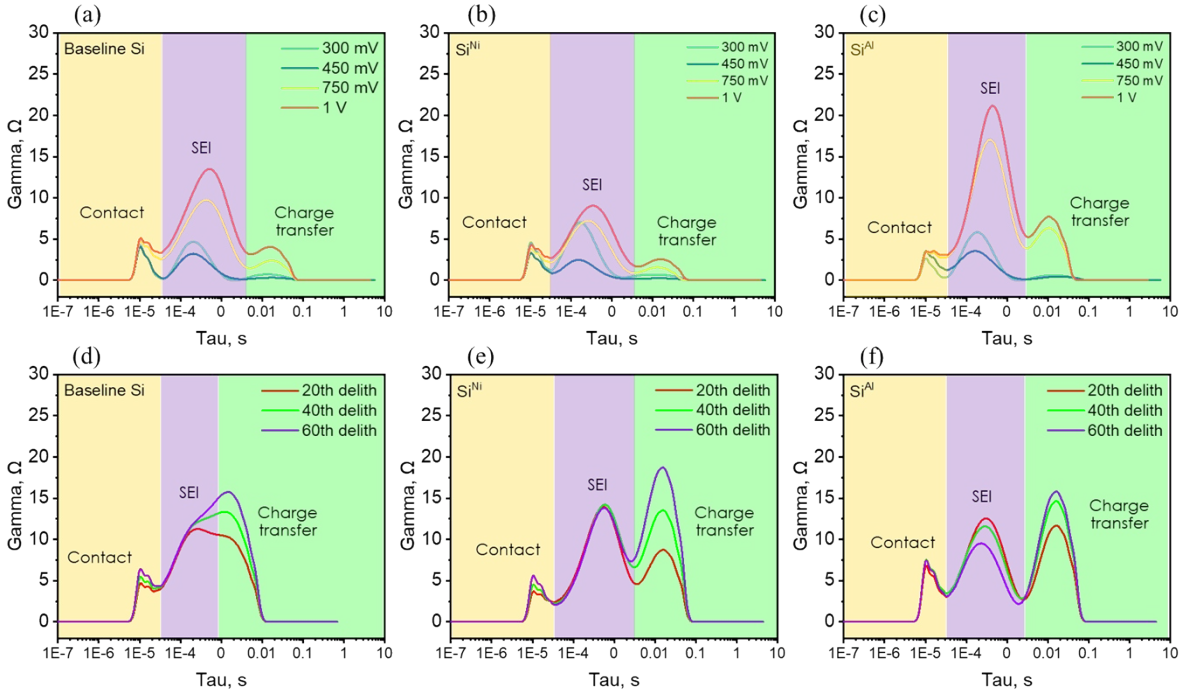


**Figure S6.** Distribution of relaxation times (DRT) plots at different potentials during the first delithiation of a) baseline Si, b) $Si^{Ni}$, and c) $Si^{Al}$, and DRT plots during cycling at delithiated states (delithiated at 1V) of d) baseline Si, e) $Si^{Ni}$, and f) $Si^{Al}$.

## XPS Analysis of the Electrodes

**Table S5.** Surface composition (at %) of the baseline Si electrode at different lithiation and delithiation potentials

| | Li | F | O | C | Si | P | N |
|---|---|---|---|---|---|---|---|
| 250 mV | 38.5 | 29.2 | 18.7 | 11.5 | 1.1 | 0.8 | 0.1 |
| 100 mV | 32.8 | 35.2 | 9.6 | 17.9 | 3 | 1 | 0.6 |
| 50 mV | 37.1 | 35.9 | 11 | 12.9 | 2 | 0.9 | 0.2 |
| 300 mV | 36.2 | 36.7 | 9.8 | 14.5 | 1.7 | 0.8 | 0.3 |
| 450 mV | 37.7 | 35.1 | 13.2 | 12.8 | 0 | 0.8 | 0.3 |
| 750 mV | 34.9 | 20.1 | 25 | 18.9 | 0 | 0.8 | 0.1 |
| 1.5 V | 36 | 23 | 21.5 | 18.3 | 0 | 0.9 | 0.1 |

**Table S6.** Surface composition (at %) of the $Si^{Ni}$ electrode at different lithiation and delithiation potentials

| | Li | F | O | C | Si | P | N | Ni |
|---|---|---|---|---|---|---|---|---|
| 250 mV | 25.9 | 28.9 | 13.8 | 22.6 | 3.8 | 3.4 | 1.4 | 0.1 |
| 100 mV | 31.6 | 35.5 | 11.6 | 16.1 | 2.1 | 2.4 | 0.6 | 0.1 |
| 50 mV | 34.7 | 19.7 | 24.8 | 19.6 | 0.1 | 0.7 | 0.1 | 0 |
| 300 mV | 35.6 | 26.6 | 18.5 | 17.6 | 0.3 | 1.2 | 0.2 | 0 |

| | | | | | | | | |
|---|---|---|---|---|---|---|---|---|
| 450 mV | 35.5 | 22.5 | 22.1 | 18.9 | 0 | 0.7 | 0.2 | 0 |
| 750 mV | 37.3 | 23.8 | 20.7 | 17.2 | 0 | 0.8 | 0.1 | 0 |
| 1.5 V | 36.5 | 21.7 | 22.7 | 18.2 | 0 | 0.8 | 0.1 | 0 |

**Table S7.** Surface composition (at %) of the $Si^{Al}$ electrode at different lithiation and delithiation potentials

| | Li | F | O | C | Si | P | N | Al |
|---|---|---|---|---|---|---|---|---|
| 250 mV | 24.3 | 30.8 | 12.2 | 26.8 | 2.6 | 0.9 | 1.3 | 1.2 |
| 100 mV | 37.1 | 38.7 | 8.7 | 12.5 | 2.2 | 0.0 | 0.6 | 0.3 |
| 50 mV | 38.0 | 33.8 | 14.9 | 12.3 | 0.1 | 0.0 | 0.7 | 0.1 |
| 300 mV | 36.1 | 32.9 | 12.9 | 17.0 | 0.0 | 0.0 | 0.7 | 0.2 |
| 450 mV | 28.7 | 14.1 | 21.0 | 35.3 | 0.0 | 0.5 | 0.2 | 0.1 |
| 750 mV | 36.3 | 23.6 | 22.3 | 17.2 | 0.0 | 0.3 | 0.1 | 0.2 |
| 1.5 V | 34.1 | 16.0 | 28.2 | 20.9 | 0.0 | 0.5 | 0.1 | 0.1 |

## Electrochemical Performance of $Si^{M}$ in Full Cells

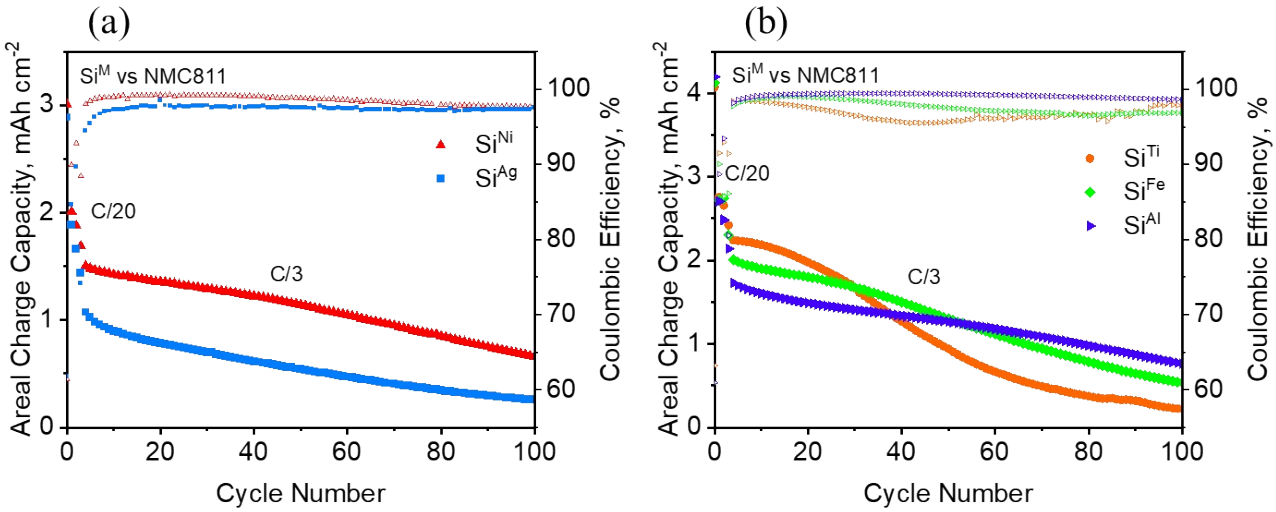


**Figure S7.** Full cell cycling behavior of select $Si^{M}$ with NMC811 with an areal loading of a) 2.59 mAh $cm^{-2}$ and b) 4.0 mAh $cm^{-2}$

## References:

(1) Többens, D. M.; Stüßer, N.; Knorr, K.; Mayer, H. M.; Lampert, G. E9: The New High-Resolution Neutron Powder Diffractometer at the Berlin Neutron Scattering Center. *Materials Science Forum* **2001**, *378-381*, 288-293. DOI: 10.4028/www.scientific.net/MSF.378-381.288.

(2) S, S.; K, A.; Dzubinska, A.; Reiffers, M.; R, N. Systematic investigations on the magnetic properties of moderate heavy Fermion CeAg0.68Si1.32 alloy. *Physica B: Condensed Matter* **2019**, *575*. DOI: 10.1016/j.physb.2019.411679.
(3) Didier, C.; Pang, W. K.; Guo, Z.; Schmid, S.; Peterson, V. K. Phase Evolution and Intermittent Disorder in Electrochemically Lithiated Graphite Determined Using in Operando Neutron Diffraction. *Chemistry of Materials* **2020**, *32* (6), 2518-2531. DOI: 10.1021/acs.chemmater.9b05145.
(4) Kohlhaas, R.; Ph., D.; Schmitz-Pranghe, N. Uber die temperaturabhangigkeit der gitterparameter von eisen, kobalt und nickel im bereich hoher temperaturen Locality: synthetic Sample: at T = 520 C. 1967.
(5) Conway, J. O.; Prior, T. J. Interstitial nitrides revisited – A simple synthesis of M Mo3N (M = Fe, Co, Ni). *Journal of Alloys and Compounds* **2019**, *774*, 69-74. DOI: 10.1016/j.jallcom.2018.09.307.
(6) Wasilewski, R. J. Thermal expansion of titanium and some titanium oxygen alloys. In Transactions of the Metallurgical Society of Aime, 1961.
(7) Spedding, F. H.; Hanak, J. J.; Daane, A. H. High temperature allotropy and thermal expansion of the rare-earth metals. *Journal of the Less Common Metals* **1961**, *3* (2), 110-124. DOI: https://doi.org/10.1016/0022-5088(61)90003-0.